

Questionable van der Waals Epitaxy of Non-Layered Materials on Fluorophlogopite Mica: The Case of ScN

Susmita Chowdhury,^{1,*} Faezeh Alijan Farzad Lahiji,^{1,2,3} Mikael Ottoson,¹ Olivier Donzel-Gargand,⁴ Robert J. W. Frost,⁵ Martin Magnuson,² Ganpati Ramanath,^{1,6,7} Arnaud le Febvier,¹ and Per Eklund^{1,2,7,*}

¹*Inorganic Chemistry, Department of Chemistry - Ångström Laboratory, Uppsala University, Box 538, SE-751 21 Uppsala, Sweden*

²*Thin Film Physics Division, Department of Physics, Chemistry and Biology (IFM), Linköping University, SE-581 83 Linköping, Sweden*

³*Materials Chemistry, RWTH Aachen University, Kope. 10, D-52074, Aachen, Germany*

⁴*Division of Solar Cell Technology, Department of Materials Science and Engineering, Uppsala University, SE-751 21 Uppsala, Sweden*

⁵*Applied Nuclear Physics, Department of Physics and Astronomy, Uppsala University, SE-751 21 Uppsala, Sweden*

⁶*Department of Materials Science and Engineering, Rensselaer Polytechnic Institute, Troy, NY 12180, USA*

⁷*Wallenberg Initiative Materials Science for Sustainability, Department of Chemistry, Uppsala University, 751 21 Uppsala, Sweden*

* Corresponding authors: susmita.chowdhury@kemi.uu.se, per.eklund@kemi.uu.se

Abstract

Growing stress-free epitaxial films by van der Waals epitaxy (vdWE) is of interest for realizing flexible optoelectronics and energy conversion devices from freestanding materials released from substrates that template epitaxy. Often, vdWE is presumed on substrates with layers held together by vdW bonding, e.g., mica, without sufficient theoretical basis or experimental evidence. Here, in case of NaCl metal nitrides, we demonstrate the thin film growth of single-domain ScN(111) by conventional epitaxy on fluorophlogopite mica(001) by sputter deposition. X-ray diffraction and electron microscopy reveal that the film/substrate epitaxial relationship is specified by $[\bar{1}01](111)_{\text{ScN}} \parallel [010](001)_{\text{mica}}$. The strong dependence of the (111) interplanar spacings with film thickness crystals indicates compressive stress buildup, which rules out the possibility of vdWE. These results are contrary to, and refute, prior claims of vdWE of non-layered metal nitrides on mica. Our findings suggest that conventional epitaxy

should be the default assumption for non-layered materials unless conditions for vdWE are explicitly established.

There is a great interest in van der Waals epitaxy (vdWE) of organic and inorganic films on substrates of layered materials held together by vdW bonding, e.g., graphene, mica, hexagonal boron nitride, and molybdenum disulfide¹⁻³. Films with weak film-substrate bonding^{2,4} and near-zero strain are key features of vdWE besides strong in-plane and out-of-plane textures. Unlike conventional epitaxy which involves strong interface bonds that lead to stress buildup with increasing film thickness, and interface dislocations above a critical epilayer thickness, vdWE offers the potential to realize thick epilayers without dislocation generation. Moreover, films grown by vdWE can be easily released from the substrate for transfer to other substrates or used as free-standing films for applications⁵. The distinguishing features of vdWE are the insensitivity of film strain to film thickness and film-surface interface bonding^{6,7}. Claims of vdWE without establishing this requirement has raised concerns² about the validity of vdWE.

Till date, vdWE has been largely been demonstrated only for substrates of 2D layered materials^{5,8,9} where sp^2 bonded layers are held by weak vdW bonding. Realizing freestanding films of non-layered rocksalt structured transition metal nitrides by vdWE has generated interest because of the exciting optoelectronic and magnetic properties^{3,10,11} of these materials. However, these metal nitrides feature covalent, ionic and/or metallic bonds^{12,13} from the sp^3d^2 electronic structure which would favor conventional epitaxy. Despite this, vdWE has been presumed or claimed on layered substrates featuring vdW bonds. Thus, the question still remains open as to whether or not vdWE can be achieved for non-layered metal nitrides on layered substrates.

Here, we demonstrate that rocksalt ScN grows on fluorophlogopite mica (f-mica, c2/m space group) by conventional epitaxy. ScN has attractive thermoelectric and piezoelectric^{14,15} and plasmonic properties¹⁶ for harvesting waste heat and mechanical energy into electrical energy. Monoclinic f-mica is a mechanically flexible substrate with high thermal stability between -100°C to 1100°C and chemical stability against concentrated acids (e.g., HCl and H₂SO₄), and transparent in the UV to IR range [Continental Trade, Warszawa, Poland]. This variant of mica specified by KMg₃(AlSi₃O₁₀)F₂ has a higher purity, thermal stability¹⁷ and mechanical stability than the traditional muscovite mica^{4,18}. Notably, mica is also known to be used for prevention of battery fires in electric cars. Moreover, f-mica exhibits ionic and covalent bonding within layers of (SiAl)O₄ tetrahedra and Mg(OF)₆ octahedra (rather than classical sp^2 bonding), and vdW bonding between the *00l* basal plane of K atoms and the (SiAl)O₄/Mg(OF)₆/(SiAl)O₄ stack¹⁹.

ScN thin films with thicknesses between \sim 8 to \sim 132 nm was grown by direct-current magnetron sputter deposition on f-mica ($00l$) surfaces freshly exfoliated by scotch tape. The substrate temperature was maintained at \sim 800°C. The substrate holder was rotated at 15 rpm for homogeneous film deposition. A 2-inch 99.9% pure Sc target was sputtered using a 110 W plasma generated by 13 sccm Ar and 31 sccm N₂ gas mixture at \approx 0.25 Pa. Prior to deposition, the system was degassed to \leq 1.3 \times 10⁻⁶ Pa. The deposition time was adjusted to achieve desired film thicknesses. X-ray reflectivity measurements were carried out to determine the thicknesses of the ScN thin films [see section S1 of the supporting information (SI)]²⁰.

Time-of-flight Elastic Recoil Detection Analysis (ToF-ERDA) measurements were carried out on thickest ScN film using a 44 MeV I¹⁰⁺ ion beam incident on the sample surface at 22.5° with the gas ionization detector placed at a 45° angle to the incidence beam to detect recoil atoms. Our analysis used POTKU software²¹ to identify elemental concentrations. Fitting details of ToF-ERDA depth profiles have been discussed in SI Section S3²⁰.

Symmetric Bragg-Brentano ω -2θ X-ray diffractograms (XRD) with ω =2θ/2 were acquired using CuK_α radiation powered by 40 mA at 45 kV in an Empyrean, Malvern Panalytical system with multicore optics. The incident beam passed through a 1/4° divergence slit and a Ni filter, and the diffracted beam was detected using a PIXcel 1D detector. The step size $\Delta\theta$ =0.02° and the counting time per step was 197 s. High-resolution X-ray diffractograms around the (111) and (222) reflections, and ω scans around the 111 peaks, were obtained using a Malvern Panalytical X'Pert Materials Research diffractometer with CuK_{α1} source. The detection mode was in scanning line for θ-2θ scan and a receiving slit with a resolution of 0.02° was used for ω scans. Pole figure scans for ScN{111} reflections were acquired for 2θ=34.35° to confirm ScN epitaxy on f-mica [Supplemental Information (SI), Section S2]. As the superimposed poles from the substrates and film were difficult to distinguish, we also acquired ϕ scans in a Malvern Panalytical X'Pert MRD system with a 4 \times 4 mm² spot. The point-focused incident beam passed through poly capillary optics and crossed slits, and the diffracted beam was collected by a proportional detector. The X-ray diffractograms along the { $\bar{1}$ 11} planes were also acquired at $\psi \neq 0^\circ$ for 2θ \sim 34°.

Scanning transmission electron microscopy (STEM) was carried out at 200 kV in a Titan Themis200 on sample cross-section prepared by focused ion beam milling. To protect the sample from possible beam damages, it was first coated with carbon. To improve its conductivity and reduce possible charging during the preparation of the lamella, the whole

surface was coated with AuPd. The lamella was cut and extracted in a Crossbeam550 from Zeiss and polished in an Helios5 from Thermo Fisher. Ga-ions were used for the polishing with specific care for the final steps, gradually decreasing the ion accelerating voltage down to 5, 2 and 1 kV to reduce as much as possible ion-implantation and beam damages.

ToF-ERDA results indicate stoichiometric ScN film seen from an elemental ratio of N/Sc = 0.97 ± 0.01 that is 1 within the error bars. Adventitious impurities include ~ 5 at.% oxygen in the film due to low enthalpy of formation of Sc-O bonds²², and ~ 5 at. % carbon at the film-substrate interface (see SI Section S3)²⁰. Contamination from scotch tape used to delaminate mica prior to ScN deposition could be a contributor to the latter.

X-ray diffractograms from ScN films showed Bragg peaks showed out-of-plane 111 and (222) reflections besides substrate f-mica(001) reflections (Figure 1a), indicating ScN(111) planes stacked along the [111] direction. High-resolution scans (see Figure 1b) reveal a monotonic decrease in (111) and (222) interplanar spacings d_{111} and d_{222} with increasing film thickness (see Figure 1c). The d_{222} value for the thinnest ScN film could not be accurately ascertained due to the large peak width. Thicker (*e.g.*, 13-132 nm) ScN films exhibit $2.604 \pm 0.004 \leq d_{111} \leq 2.632 \pm 0.006$ Å range and $1.302 \pm 0.004 \leq d_{222} \leq 1.305 \pm 0.005$ Å.

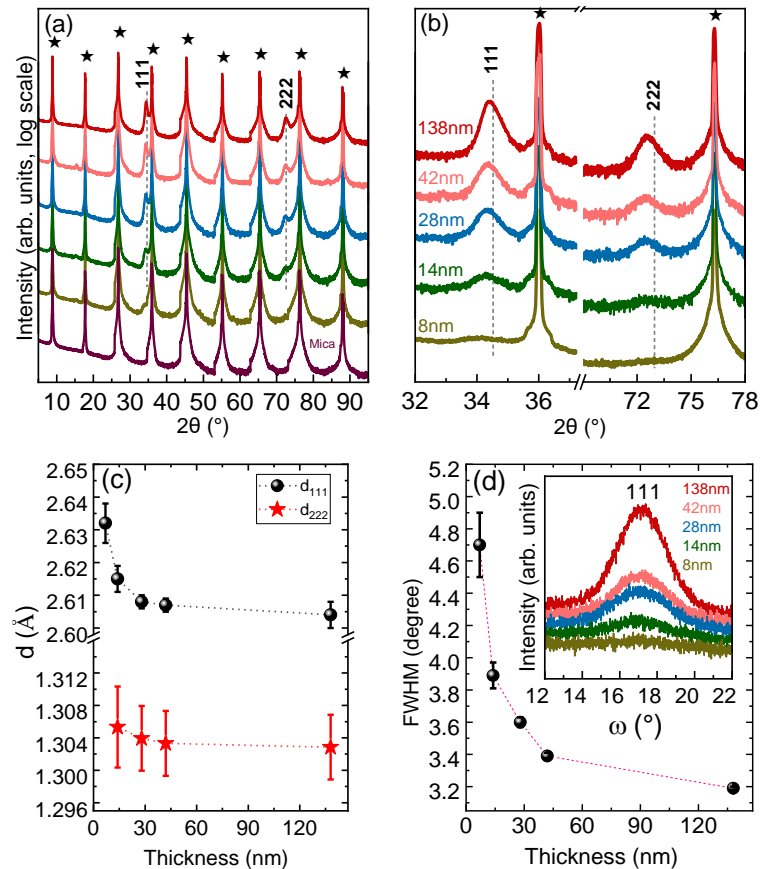


Figure 1. Representative X-ray diffractograms (a) with a Cu K α beam and (b) high-resolution scans obtained from ScN films of different film thicknesses on f-mica. (c) Interplanar spacings of 111 and 222, d_{111} and d_{222} plotted versus ScN film thickness t_{film} . (d) Full-width-at-half-maximum (FWHM) of the 111 peak plotted versus t_{film} using data from ω scan rocking curves (inset).

The ScN(111) peak width determined from rocking curve ω -scans decreases with increasing film thicknesses (Figure 1d). The rocking curves were measured for 111 peaks. The high full-width half-maximum peak width of $\sim 3.19^\circ$ even for the thickest ScN film could be from misoriented crystal domains and high defect density. Peak width gradually decreases from 4.7° (± 0.2) to 3.39° (± 0.02) with increasing film thickness, suggesting domain coalescence and defect annihilation.

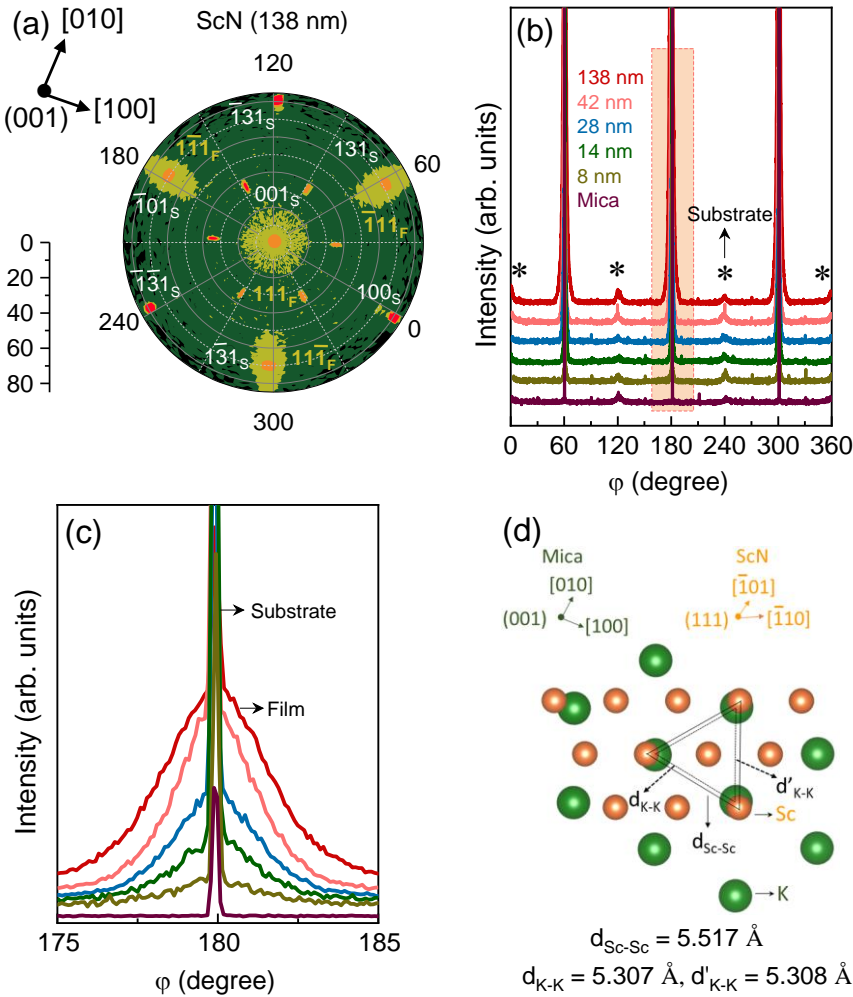


Figure 2. (a) Pole figure scan of the ScN(111) reflection with $2\theta = 34.35^\circ$ from the thickest ScN film. (b) ϕ scans showing the ScN(111) pole peaks and the f-mica(001) substrate peaks. (c) A

magnified view of ϕ scans around $\phi \approx 180^\circ$ depicting the high width of ScN(111) poles films in contrast to the narrow pole from the f-mica(001) substrate. (d) Schematic sketches depicting atomic registry between epitaxial ScN(111) and f-mica (001) with green spheres depicting K in mica and red spheres showing Sc in ScN.

Pole figures from the thickest ScN film (Figure 2a) measured at $2\theta = 34.35^\circ$ show several sets of poles and one set of pole clusters as a result of diffraction from both substrate and film. Two different sets of poles can be observed, (i) sharp spotty poles and (ii) broad features at $\psi = 0^\circ$ and at $\sim 70^\circ$. To distinguish the substrate and film contribution, azimuthal ϕ scans of the poles from ScN films and bare f-mica at $\psi \sim 70^\circ$ (Figure 2b) were performed and a magnified view around $\phi \sim 180^\circ$ confirm broad ScN poles with $\Delta\phi \sim \pm 5^\circ$ (Figure 2c). This is in contrast to the narrow poles from f-mica: 131, $\bar{1}01$ and $1\bar{3}1$ that are intense, and $\bar{1}31$, $\bar{1}\bar{3}1$ and 100 that are faint which can be attributed combining pole figure and ϕ scans. The result is consistent with high peak width of ScN(111) likely arising from crystal mosaicity and defects. Thus, in pole figure (Figure 2a), the central pole cluster around at $\psi = \phi = 0^\circ$ connotes ScN(111) and that around $\psi \sim 70^\circ$ and $\phi \approx 60^\circ, 180^\circ$ and 300° correspond to $\bar{1}11$, $1\bar{1}1$ and $11\bar{1}$. The six other poles at $\psi \sim 34.7^\circ$ separated by $\Delta\phi \approx 60^\circ$. The three poles at $\psi \sim 71^\circ$ and three at $\psi \sim 79^\circ$ with $\Delta\phi \approx 120^\circ$ arise from f-mica (see SI Figure S2)²⁰.

The threefold symmetry of ScN{111} poles suggest that ScN(111) is related epitaxially to f-mica(001) by $[\bar{1}01](111)_{\text{ScN}} \parallel [010](001)_{\text{mica}}$. This is captured by the atomistic registry through a schematic sketch of the atomic arrangement of a ScN(111) crystal on mica(001) (Figure 2d). For simplification, only K atoms from mica(001) planes¹⁹ and Sc atoms from ScN(111) planes were represented and allows determination of lattice mismatch. The crystal structure of f-mica and bulk ScN were adopted from PCPDF #04-009-4162 (f-mica: $a = 5.307 \text{ \AA}$, $b = 9.195 \text{ \AA}$, $c = 10.134 \text{ \AA}$, $\beta = 100.08^\circ$) and #04-001-1145 (ScN: $a = b = c = 4.505 \text{ \AA}$). The interplanar lattice mismatch along the in-plane direction is $(d_{\text{K-K}} - d_{\text{Sc-Sc}}/d_{\text{K-K}}) \times 100\% \approx -3.95\%$ whereas, along the diagonal, it is $(d'_{\text{K-K}} - d_{\text{Sc-Sc}}/d'_{\text{K-K}}) \times 100\% \approx -3.78\%$. This analysis of our results indicates the presence of only a single domain with ABCABC stacking in our sputter-deposited ScN films. Due to in-plane lattice mismatch between f-mica and ScN, the first few monolayers grown in strained fashion can promote single domain growth of ScN(111) on f-mica(001). This result is contrary to reports of twin domains in ScN and TiN films grown by molecular beam epitaxy on f-mica^{11,18}, with ABCABC and ACBACB stacking sequences²³. This difference could be from

vastly different energetics of adatom interactions on the surface that could alter crystal growth evolution paths.

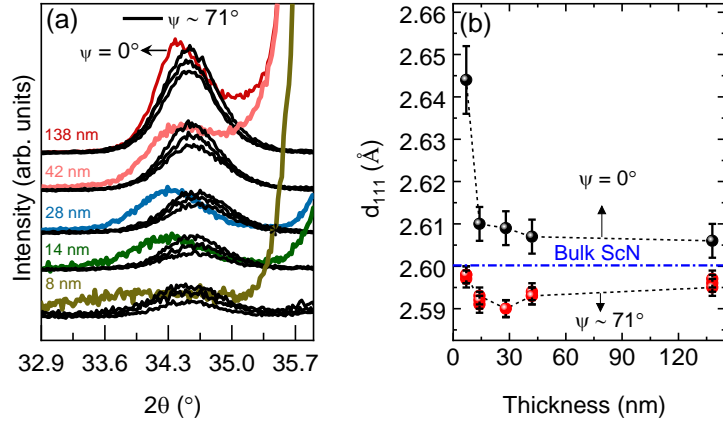


Figure 3. (a) $\text{ScN}\{111\}$ peaks from high resolution scans around $\psi = 0^{\circ}$ and three additional locations with $\psi \sim 71^{\circ}$ plotted as a function of the diffraction angle 2θ . (b) $\text{ScN}(111)$ interplanar-spacings for $\psi = 0^{\circ}$ and $\psi \sim 71^{\circ}$ plotted versus ScN film thickness t_{film} . The horizontal line depicting the bulk $\text{ScN}(111)$ interplanar spacing $d_{111} = 2.60 \text{ \AA}$ is shown for reference from PCPDF #04-001-1145.

The 2θ diffraction angles corresponding to the tilted three non-central $\{\bar{1}11\}$ planes, namely, $\bar{1}11$, $1\bar{1}1$, $1\bar{1}\bar{1}$ are similar within experimental uncertainty, but distinctly larger than that of the central out-of-plane (111) peak (Figure 3a). The extent of the difference between the interplanar spacings corresponding to non-central $\{\bar{1}11\}$ and central (111) diminishes with increasing film thickness (Figure 3b). Both the d_{111} and $d_{\{\bar{1}11\}}$ values depart from the $d = 2.600 \text{ \AA}$ value of bulk ScN adopted from PCPDF #04-001-1145. As ScN film thickness increases from 8 nm to 138 nm, the difference in d -spacing is indicative of in-plane compressive strain in the film. The decrease in the difference for higher thickness implies strain relaxation, likely due to dislocation formation.

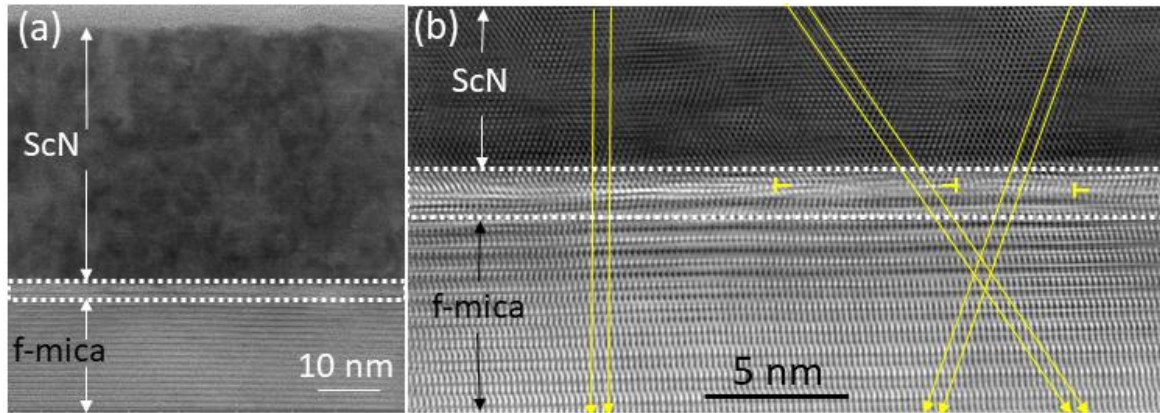


Figure 4. (a) Drift corrected frame integrated bright field STEM micrograph from a ScN(111) grown on f-mica(001). (b) Magnified view showing the atomistic details at the ScN/mica interface with \leftarrow and \rightarrow showing dislocation and appearance of extra plane while diagonal and vertical arrows show atom on atom registry *i.e.*, epitaxy.

Drift corrected frame integrated bright-field STEM reveals substrate, film and film-substrate interface intermixing region bounded by dotted white lines in Figure 4a. Examining magnified lattice images in this region (Figure 4b) shows atom on atom registry of ScN on f-mica shown by diagonal and vertical arrows, a guide to eye, confirming the epitaxial nature. Across the ScN/mica interface, rotated crystal planes away from the optic axis forms distorted contrast which results from defects in this region. Along the stacking sequence at the interface, edge dislocations (shown by \leftarrow and \rightarrow) and appearance of extra planes are identified. Presence of these defects reflects the lattice mismatch of film from the substrate and reinforces the observation made from the Bragg-Brentano measurement where compressive strain was observed reminiscent of conventional epitaxy. These results do not support vdWE which involves near-zero strain.

Layered mica substrates foster vdWE for layered materials through weak interlayer bonding²⁴ e.g., in, Bi_2X_3 ($\text{X} = \text{Te}$ and Se)²⁵, 2D hexagonal Te ²⁶, MoS_2 ²⁷, orthorhombic α - MoO_3 ²⁸ and monoclinic VO_2 ⁴. In contrast, non-layered materials generally do not exhibit vdWE on mica, as shown for cubic NaCl rocksalt NiO ²⁹, and perovskite SrTiO_3 ³⁰, hexagonal wurtzite InN ³¹, hexagonal ZnO ² and Al_2O_3 ⁹, exception being non-layered monoclinic MoO_2 ³². TMNs are another class of widespread materials known to exhibit covalent and ionic bonds between metal and N atoms while metallic bonding persists between the metals^{12,13}. Our results

collectively contradict prior claims of vdWE growth of rocksalt TiN¹¹ and ScN¹⁸ on f-mica. have been made without investigating the stress evolution as a function of epilayer thickness. In addition, the epilayer stayed intact without delaminating from the substrate under several bending cycles¹⁸ despite weak interaction energy of 10^{-1} - 10^1 kJ mol⁻¹ of vdW force compared to strong (10^2 - 10^3 kJ mol⁻¹) covalent and ionic bonds³³ known to exhibit in transition metal nitrides which further opens the question if utilizing Van der Waals material as a substrate can ensure quasi vdWE to a non-layered overlayer. Our results on the other hand clearly show that ScN(111) interplanar spacings are very sensitive to epilayer thickness, indicative of conventional epitaxy. The lack of examination of film stress development as a function of epilayer thickness in the earlier studies is the likely reason for erroneous attribution of vdWE. We thus propose that conventional epitaxy should be the default assumption rather be that vdWE for non-layered materials on mica unless there is compelling evidence of insensitivity of interplanar spacing with film thickness.

In summary, sputter-deposited ScN thin films on f-mica exhibit conventional epitaxy rather than vdWE. In particular, we find ScN crystals grow in a single-domain epitaxy specified by $[\bar{1}01](111)_{\text{ScN}}||[010](001)_{\text{mica}}$. This is contrary to twin domain growth of TiN and ScN epilayers by molecular beam epitaxy, indicating that adatom interactions on the surface can have a significant effect on crystal growth evolution. The presence of significant compressive strain in the ScN films, and its sensitivity to epilayer thickness refutes vdWE. These results persuade us to conclude that conventional epitaxy should be the default assumption for non-layered materials on mica substrate, unless compelling evidence of strain insensitivity with epilayer thickness. Our results shown for ScN should be applicable to other NaCl transition metal nitrides and oxides with non-layered crystal structures.

Acknowledgements

The authors acknowledge funding from the Swedish Government Strategic Research Area in Materials Science on Functional Materials at Linköping University (Faculty Grant SFO-Mat-LiU No. 2009 00971), the Knut and Alice Wallenberg foundation through the Wallenberg Academy Fellows program (KAW-2020.0196), the Swedish Research Council (VR) under Project No. 2021-03826, 2025-03680 (PE), 2025-03760 (AF), 2025-03705 (MM) and 2024-04996 (GR). MM acknowledges financial support from the Swedish Energy Agency (Grant No. 43606-1) and the Carl Tryggers Foundation (CTS 25:3972, CTS23:2746, CTS20:272). SC thanks Erik Lewin for fruitful discussions and Sanath Kumar Honnali for his help during pole figure measurement. GR acknowledges support from the Wallenberg Initiative Materials Science for Sustainability (WISE) funded by the Knut and Alice Wallenberg Foundation, the US NSF grant CMMI 2135725 through the BRITE program, the Empire State Development's Division of Science, Technology and Innovation Focus Center at RPI (C210117).

References

- (1) Novoselov, K. S.; Mishchenko, A.; Carvalho, A.; Castro Neto, A. H. 2D Materials and van Der Waals Heterostructures. *Science* **2016**, *353* (6298), aac9439. <https://doi.org/10.1126/science.aac9439>.
- (2) Wang, N.; Pan, X.; Wang, P.; Wang, Y.; He, H.; Zeng, Y. J.; Zhang, L.; Li, Y.; Wang, F.; Lu, B.; Huang, J.; Ye, Z. Is All Epitaxy on Mica van Der Waals Epitaxy? *Mater. Today Nano* **2022**, *20*, 100255. <https://doi.org/10.1016/j.mtnano.2022.100255>.
- (3) Kim, J.; Bayram, C.; Park, H.; Cheng, C. W.; Dimitrakopoulos, C.; Ott, J. A.; Reuter, K. B.; Bedell, S. W.; Sadana, D. K. Principle of Direct van Der Waals Epitaxy of Single-Crystalline Films on Epitaxial Graphene. *Nat. Commun.* **2014**, *5* (1), 4836. <https://doi.org/10.1038/ncomms5836>.
- (4) Ekström, E.; Hurand, S.; le Febvrier, A.; Elsukova, A.; Persson, P. O. Å.; Paul, B.; Eriksson, F.; Sharma, G.; Voznyy, O.; Sangiovanni, D. G.; Ramanath, G.; Eklund, P. Microstructure Control and Property Switching in Stress-Free van Der Waals Epitaxial VO₂ Films on Mica. *Mater. Des.* **2023**, *229*, 111864. <https://doi.org/10.1016/j.matdes.2023.111864>.
- (5) Duong, D. L.; Yun, S. J.; Lee, Y. H. Van Der Waals Layered Materials: Opportunities and Challenges. *ACS Nano*. **2017**, *11* 1803. <https://doi.org/10.1021/acsnano.7b07436>.
- (6) Vermeulen, P. A.; Mulder, J.; Momand, J.; Kooi, B. J. Strain Engineering of van Der Waals Heterostructures. *Nanoscale* **2018**, *10* (3), 1474–1480. <https://doi.org/10.1039/c7nr07607j>.
- (7) Zhang, H.; Kooi, B. J.; Yimam, D. T.; De Graaf, S.; Momand, J.; Vermeulen, P. A.; Wei, Y.; Noheda, B. Strain Relaxation in “2D/2D and 2D/3D Systems”: Highly Textured Mica/Bi₂Te₃, Sb₂Te₃/Bi₂Te₃, and Bi₂Te₃/GeTe Heterostructures. *ACS Nano* **2021**, *15* (2), 2869–2879. <https://doi.org/10.1021/acsnano.0c08842>.
- (8) Xie, C.; Mak, C.; Tao, X.; Yan, F. Photodetectors Based on Two-Dimensional Layered Materials Beyond Graphene. *Adv. Funct. Mater.* **2017**, *27* (19), 1603886. <https://doi.org/10.1002/adfm.201603886>.
- (9) Steinberg, S.; Ducker, W.; Vigil, G.; Hyukjin, C.; Frank, C.; Tseng, M. Z.; Clarke, D. R.; Israelachvili, J. N. Van Der Waals Epitaxial Growth of α -Alumina Nanocrystals on Mica.

Science 1993, 260 (5108), 656.

<https://doi.org/https://doi.org/10.1126/science.260.5108.656>.

(10) Patsalas, P.; Kalfagiannis, N.; Kassavetis, S.; Abadias, G.; Bellas, D. V.; Lekka, C.; Lidorikis, E. Conductive Nitrides: Growth Principles, Optical and Electronic Properties, and Their Perspectives in Photonics and Plasmonics. *Materials Science and Engineering R: Reports* **2018**, *123*, 1–55. <https://doi.org/10.1016/j.mser.2017.11.001>.

(11) Zhang, R.; Li, X.; Meng, F.; Bi, J.; Zhang, S.; Peng, S.; Sun, J.; Wang, X.; Wu, L.; Duan, J.; Cao, H.; Zhang, Q.; Gu, L.; Huang, L. F.; Cao, Y. Wafer-Scale Epitaxy of Flexible Nitride Films with Superior Plasmonic and Superconducting Performance. *ACS Appl. Mater. Interfaces* **2021**, *13* (50), 60182. <https://doi.org/10.1021/acsami.1c18278>.

(12) Oyama, S. *Introduction to the Chemistry of Transition Metal Carbides and Nitrides*; Springer, 1996.

(13) Chen, J. G. Carbide and Nitride Overlays on Early Transition Metal Surfaces: Preparation, Characterization, and Reactivities. *Chem. Rev.* **1996**, *96* (4), 1477. <https://doi.org/https://doi.org/10.1021/cr950232u>.

(14) Burmistrova, P. V.; Maassen, J.; Favaloro, T.; Saha, B.; Salamat, S.; Rui Koh, Y.; Lundstrom, M. S.; Shakouri, A.; Sands, T. D. Thermoelectric Properties of Epitaxial ScN Films Deposited by Reactive Magnetron Sputtering onto MgO(001) Substrates. *J. Appl. Phys.* **2013**, *113* (15), 153704. <https://doi.org/10.1063/1.4801886>.

(15) Akiyama, M.; Kamohara, T.; Kano, K.; Teshigahara, A.; Takeuchi, Y.; Kawahara, N. Enhancement of Piezoelectric Response in Scandium Aluminum Nitride Alloy Thin Films Prepared by Dual Reactive Cospattering. *Advanced Materials* **2009**, *21* (5), 593–596. <https://doi.org/10.1002/adma.200802611>.

(16) Maurya, K. C.; Rao, D.; Acharya, S.; Rao, P.; Pillai, A. I. K.; Selvaraja, S. K.; Garbrecht, M.; Saha, B. Polar Semiconducting Scandium Nitride as an Infrared Plasmon and Phonon-Polaritonic Material. *Nano Lett.* **2022**, *22* (13), 5182–5190. <https://doi.org/10.1021/acs.nanolett.2c00912>.

(17) Islam, M. R.; Tomitori, M. Evaluation of the Discrete Thickness of Exfoliated Artificially Synthesized Mica Nanosheets on Silicon Substrates: Toward Characterization of the Tunneling Current through the Nanosheets. *Appl. Surf. Sci.* **2020**, *532*, 147388. <https://doi.org/10.1016/j.apsusc.2020.147388>.

(18) Mukhopadhyay, D.; Rao, D.; Rawat, R. S.; Indiradevi, A.; Pillai, K.; Garbrecht, M.; Saha, B. Flexible Near-Infrared Plasmon-Polaritons in Epitaxial Scandium Nitride Enabled by van Der Waals Heteroepitaxy. *Nano Lett.* **2024**, *24* (45), 14493. <https://doi.org/10.1021/acs.nanolett.4c04616>.

(19) Lu, L.; Dai, Y.; Du, H.; Liu, M.; Wu, J.; Zhang, Y.; Liang, Z.; Raza, S.; Wang, D.; Jia, C. L. Atomic Scale Understanding of the Epitaxy of Perovskite Oxides on Flexible Mica Substrate. *Adv. Mater. Interfaces* **2020**, *7* (2), 1901265. <https://doi.org/10.1002/admi.201901265>.

(20) Chowdhury, S.; Lahiji, F. A. F.; Ottoson, M.; Gargand, O. D.; Frost, R.; Magnuson, M.; Ramanath, G.; Fevrier, A. le; Eklund, P. Questionable van Der Waals Epitaxy of Non-Layered Materials on Fluorophlogopite Mica: The Case of ScN, Supporting Information. *XXXXX* **2026**.

(21) Arstila, K.; Julin, J.; Laitinen, M. I.; Aalto, J.; Konu, T.; Kärkkäinen, S.; Rahkonen, S.; Raunio, M.; Itkonen, J.; Santanen, J. P.; Tuovinen, T.; Sajavaara, T. Potku - New Analysis Software for Heavy Ion Elastic Recoil Detection Analysis. *Nucl. Instrum. Methods Phys. Res. B* **2014**, *331*, 34–41. <https://doi.org/10.1016/j.nimb.2014.02.016>.

(22) Chowdhury, S.; Gupta, R.; Rajput, P.; Tayal, A.; Rao, D.; Sekhar, R.; Prakash, S.; Rajagopalan, R.; Jha, S. N.; Saha, B.; Gupta, M. Detailed Study of Reactively Sputtered ScN Thin Films at Room Temperature. *Materialia* **2022**, *22*, 101375. <https://doi.org/10.1016/j.mtla.2022.101375>.

(23) Sandström, S.; Svedberg, E. B.; Birch, J.; Sundgren, J.-E. Structure and Surface Morphology of Epitaxial Ni Films Grown on MgO(111) Substrates: Growth of High Quality Single Domain Films. *J. Cryst. Growth* **1999**, *197* (4), 849–857. [https://doi.org/https://doi.org/10.1016/S0022-0248\(98\)00972-5](https://doi.org/https://doi.org/10.1016/S0022-0248(98)00972-5).

(24) Frisenda, R.; Niu, Y.; Gant, P.; Muñoz, M.; Castellanos-Gomez, A. Naturally Occurring van Der Waals Materials. *NPJ 2D Mater. Appl.* **2020**, *4* (1), 38. <https://doi.org/10.1038/s41699-020-00172-2>.

(25) Li, H.; Cao, J.; Zheng, W.; Chen, Y.; Wu, D.; Dang, W.; Wang, K.; Peng, H.; Liu, Z. Controlled Synthesis of Topological Insulator Nanoplate Arrays on Mica. *J. Am. Chem. Soc.* **2012**, *134* (14), 6132–6135. <https://doi.org/10.1021/ja3021395>.

(26) Wang, Q.; Safdar, M.; Xu, K.; Mirza, M.; Wang, Z.; He, J. Van Der Waals Epitaxy and Photoresponse of Hexagonal Tellurium Nanoplates on Flexible Mica Sheets. *ACS Nano* **2014**, *8* (7), 7497–7505. <https://doi.org/10.1021/nn5028104>.

(27) Wang, Y.; Chen, Z.; Deschler, F.; Sun, X.; Lu, T. M.; Wertz, E. A.; Hu, J. M.; Shi, J. Epitaxial Halide Perovskite Lateral Double Heterostructure. *ACS Nano* **2017**, *11* (3), 3355–3364. <https://doi.org/10.1021/acsnano.7b00724>.

(28) Lahiji, F. A. F.; Paul, B.; Le Febvrier, A.; Ramanath, G. Van Der Waals Epitaxy of α -MoO₃ Films on f-Mica by Pulsed Sputter Deposition. *arXiv preprint arXiv:2502.10594* **2025**.

(29) A.F. Lahiji, F.; Paul, B.; le Febvrier, A.; Eklund, P. Conventional Epitaxy of NiO Thin Films on Muscovite Mica and C-Al₂O₃ Substrates. *Thin Solid Films* **2024**, *808*, 140566. <https://doi.org/10.1016/j.tsf.2024.140566>.

(30) Liang, R.; Ke, S. The Competition between van Der Waals and Ionic Interactions at the SrTiO₃/Mica Heterointerface. *Appl. Phys. Lett.* **2025**, *126* (11), 111605. <https://doi.org/10.1063/5.0260844>.

(31) Geng, Y.; Xu, Y.; Li, X.; Wang, X.; Wu, H.; Liu, C. Molecular Beam Epitaxy of Flexible InN Thin Films on Fluorophlogopite Mica. *J. Cryst. Growth* **2025**, *671*, 128355. <https://doi.org/10.1016/j.jcrysgro.2025.128355>.

(32) Ma, C. H.; Lin, J. C.; Liu, H. J.; Do, T. H.; Zhu, Y. M.; Ha, T. D.; Zhan, Q.; Juang, J. Y.; He, Q.; Arenholz, E.; Chiu, P. W.; Chu, Y. H. Van Der Waals Epitaxy of Functional MoO₂ Film on Mica for Flexible Electronics. *Appl. Phys. Lett.* **2016**, *108* (25), 253104. <https://doi.org/10.1063/1.4954172>.

(33) Wang, P.; Jia, C.; Huang, Y.; Duan, X. Van Der Waals Heterostructures by Design: From 1D and 2D to 3D. *Matter* **2021**, *4* (2), 552–581. <https://doi.org/10.1016/j.matt.2020.12.015>.

Supporting Information

Questionable van der Waals Epitaxy of Non-Layered Materials on Fluorophlogopite Mica: The Case of ScN

Susmita Chowdhury,^{1,*} Faezeh Alijan Farzad Lahiji,^{1,2,3} Mikael Ottoson,¹ Olivier Donzel-Gargand,⁴ Robert J. W. Frost,⁵ Martin Magnuson,² Ganpati Ramanath,^{1,6,7} Arnaud le Febvrier,¹ and Per Eklund^{1,2,7,*}

¹*Inorganic Chemistry, Department of Chemistry - Ångström Laboratory, Uppsala University, Box 538, SE-751 21 Uppsala, Sweden*

²*Thin Film Physics Division, Department of Physics, Chemistry and Biology (IFM), Linköping University, SE-581 83 Linköping, Sweden*

³*Materials Chemistry, RWTH Aachen University, Kope. 10, D-52074, Aachen, Germany*

⁴*Division of Solar Cell Technology, Department of Materials Science and Engineering, Uppsala University, SE-751 21 Uppsala, Sweden*

⁵*Applied Nuclear Physics, Department of Physics and Astronomy, Uppsala University, SE-751 21 Uppsala, Sweden*

⁶*Department of Materials Science and Engineering, Rensselaer Polytechnic Institute, Troy, NY 12180, USA*

⁷*Wallenberg Initiative in Materials Science for Sustainability, Department of Chemistry, Uppsala University, 751 21 Uppsala, Sweden*

* Corresponding authors: susmita.chowdhury@kemi.uu.se, per.eklund@kemi.uu.se

S1. Thickness of the samples

The thickness of the samples was obtained from fitting of the X-ray reflectivity (XRR) data. The XRR measurements were performed on a Malvern Panalytical X'Pert Materials Research Diffractometer using CuK α X-ray radiation and 1/32° divergence slit at the incident beam optics side setting the acceleration voltage at 45kV and tube current at 20 mA. A Ni 0.15 mm beam attenuator was also used along the incident beam side setting the activate and deactivate level at 400K and 200K cps to protect the detector from high intense direct beam exposure. With a step size of 0.005°, the scanning range of 2 θ was set at 0.2°-3°. During the alignment steps of 2 θ →Z→ ω →Z→ ω → ψ → ω , the Z height was adjusted for each sample scans due to non-uniformity in exfoliation of the mica layers with the uncontrolled scotch tape procedure.

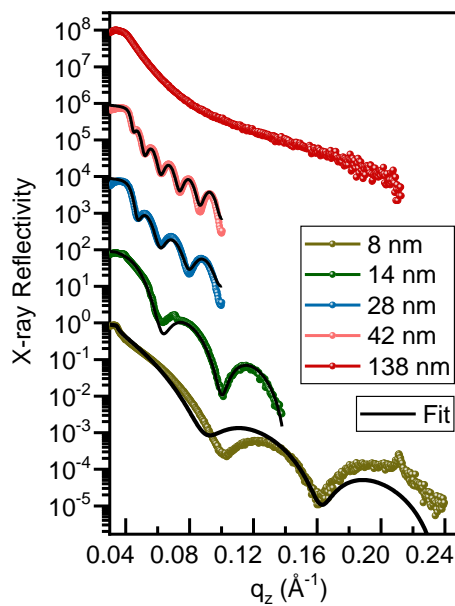


Figure S1. XRR of thickness dependent ScN thin film samples deposited on f-mica substrate.

The XRR fitting was performed using Parratt 32 software based on Parratt's formalism¹. The Kiessig fringes were observed for all the samples except the thickest sample as shown in Figure S1. The Kiessig oscillations were not apparent for the thickest sample due to detection limit of the instrument. The thicknesses obtained from the fitted spectra are 8(± 1.1) nm, 14(± 0.5) nm, 28(± 0.2) and 42(± 0.2) nm, respectively for the thinner samples and yields a deposition rate of 0.023 nm/s. Hence the thickness of the thickest sample can be estimated at ≈ 138 nm under the similar deposition conditions except variable deposition time.

S2. Pole figure of f-mica

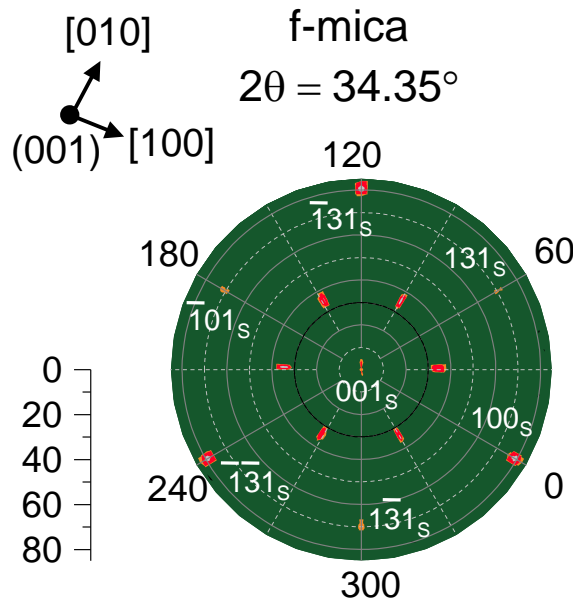


Figure S2. Pole figure in log scale of f-mica substrate.

Figure S2 shows the pole figure of f-mica measured at a similar Bragg diffraction angle $2\theta = 34.35^\circ$ to that of the ScN film. Four different set of poles were detected from the monocrystalline f-mica substrate at variable χ corresponding to different φ values. They are identified as (i) central pole appears at $\psi = \varphi = 0^\circ$: 001, (ii) six set of poles at $\psi \sim 34.7^\circ$ distributed at $\Delta\varphi \approx 60^\circ$, (iii) three set of poles at $\psi \sim 71^\circ$ and $\Delta\varphi \approx 120^\circ$: 131, $\bar{1}01$ and $\bar{1}31$ and, (iv) three intense poles at $\psi \sim 79^\circ$ and $\Delta\varphi \approx 120^\circ$: $\bar{1}31$, $\bar{1}\bar{3}1$, 100.

S3. Compositional analysis of ScN

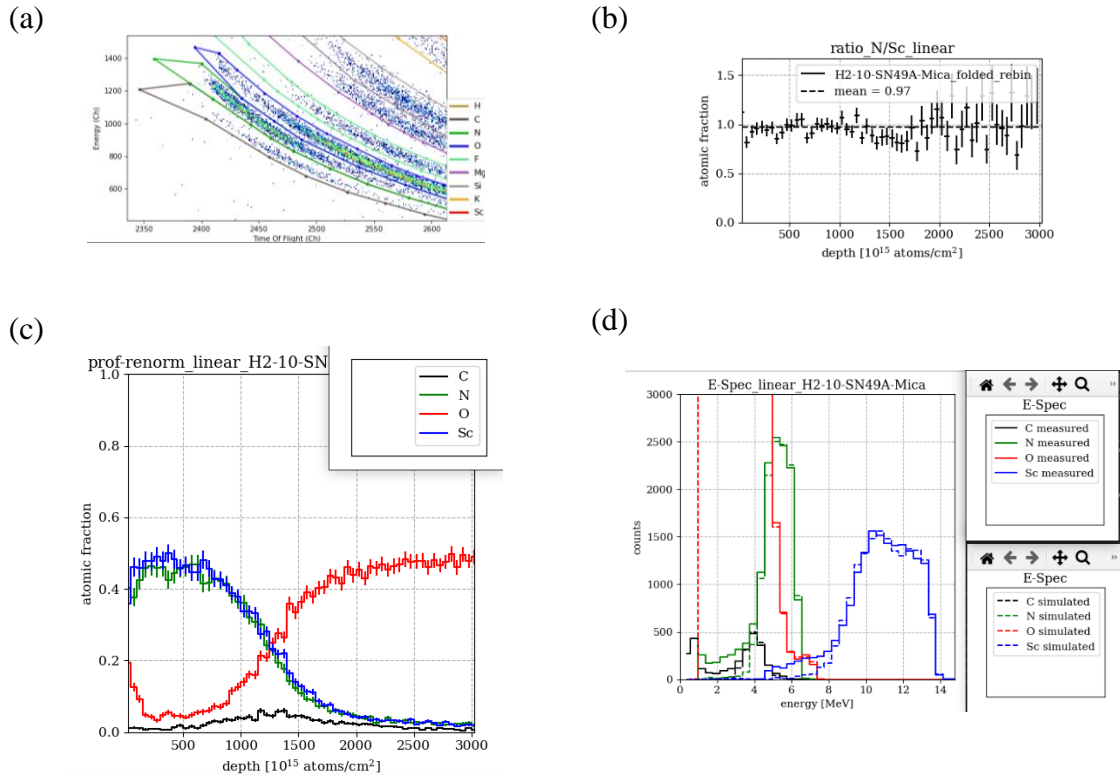


Figure S3. (a) The ToF-ERDA profiles of the constituent elements from ScN film and f-mica substrate. (b) The N/Sc ratio determined from ToF-ERDA plotted as a function of depth from the surface for the thickest ScN epilayers grown on f-mica. (c) Elemental depth profiles of Sc and N in ScN, and K, Mg, Al, Si, O and F in f-mica along with adventitious O and C. (d) The good fit of the constituent elements can be seen from the measured and simulated data.

The experimental ToF-ERDA data of the thickest ScN film is shown in Figure S3(a). Fitting the constituent elemental profiles with bananas resulted in the N/Sc ratio of 0.97 (Figure S3 b). The depth profiles of Sc and N from the ScN film and presence of unintentional O of ~5 at. % was detected within the film (Figure S3 c). At the film-substrate interface, unintentional C contaminations of ~5 at. % was also detected which could be from the use of scotch tape to delaminate the top surface layer of the substrate and expose a fresh surface for ScN deposition. The measured and simulated data of Sc, N, O and C shows the good fit of the ToF-ERDA data (Figure S3 d).

S4. Elemental distribution and diffraction pattern of ScN on f-mica

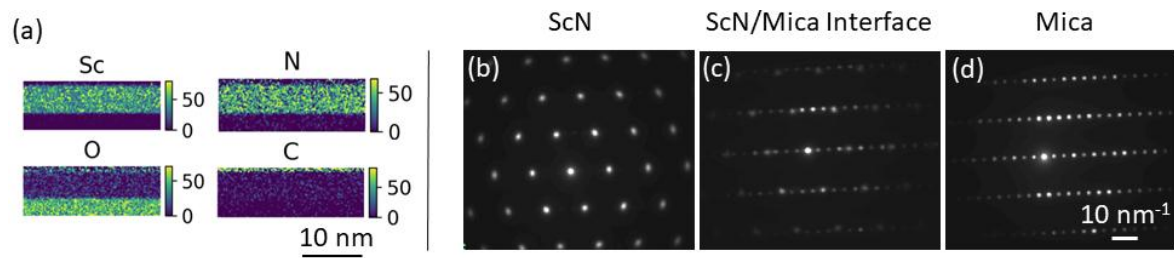


Figure S4. (a) Energy Dispersive X-ray profiles of Sc, N, and unintentional adventitious O and C. (b-d) Integrated diffraction patterns extracted from a single 4D-STEM map acquired in nanobeam diffraction. The electron diffraction patterns of (b) ScN film, (c) substrate-film interface and (d) f-mica.

Energy Dispersive X-ray Spectroscopy show a homogeneous distribution of N and Sc in the ScN film, as expected (Figure S4 a). Unintentional presence of adventitious O and C are low in the film. Spotty electron diffraction patterns from film/substrate interface (Figure S4 c) consist of superposed patterns from ScN film (Figure S4 b) and f-mica substrate (Figure S4 d), indicating crystalline nature of the interface.

Reference

- (1) Parratt, L. G. Surface Studies of Solids by Total Reflection of X-Rays. *Physical Review* **1954**, 95 (2), 359–369. <https://doi.org/10.1103/PhysRev.95.359>.